

## Stoichiometry and Physical Chemistry of Promiscuous Aggregate-Based Inhibitors

Kristin E. D. Coan and Brian K. Shoichet\*

Department of Pharmaceutical Chemistry & Graduate Group in Chemistry and Chemical Biology, 1700 Fourth Street, University of California at San Francisco, San Francisco, California 94158-2550

Received April 22, 2008; E-mail: shoichet@cgl.ucsf.edu

**Abstract:** Many false positives in early drug discovery owe to nonspecific inhibition by colloid-like aggregates of organic molecules. Despite their prevalence, little is known about aggregate concentration, structure, or dynamic equilibrium; the binding mechanism, stoichiometry with, and affinity for enzymes remain uncertain. To investigate the elementary question of concentration, we counted aggregate particles using flow cytometry. For seven aggregate-forming molecules, aggregates were not observed until the concentration of monomer crossed a threshold, indicating a “critical aggregation concentration” (CAC). Above the CAC, aggregate count increased linearly with added organic material, while the particles dispersed when diluted below the CAC. The concentration of monomeric organic molecule is constant above the CAC, as is the size of the aggregate particles. For two compounds that form large aggregates, nicardipine and miconazole, we measured particle numbers directly by flow cytometry, determining that the aggregate concentration just above the CAC ranged from 5 to 30 fM. By correlating inhibition of an enzyme with aggregate count for these two drugs, we determined that the stoichiometry of binding is about 10 000 enzyme molecules per aggregate particle. Using measured volumes for nicardipine and miconazole aggregate particles ( $2.1 \times 10^{11}$  and  $4.7 \times 10^{10}$  Å<sup>3</sup>, respectively), computed monomer volumes, and the observation that past the CAC all additional monomer forms aggregate particles, we find that aggregates are densely packed particles. Finally, given their size and enzyme stoichiometry, all sequestered enzyme can be comfortably accommodated on the surface of the aggregate.

### Introduction

High-throughput screening hit lists are dominated by false positives, many of which are due to promiscuous inhibition by colloid-like aggregates of the small molecule.<sup>1–7</sup> These submicron particles form in aqueous media, leading to sequestration and nonspecific inhibition of enzymes.<sup>8</sup> In a recent high-throughput screen, 95% of the hits showed signature aggregate behavior, representing the predominant mechanism of false positives and dwarfing the hit rate for nonaggregating, potentially specific inhibitors.<sup>9</sup> Such aggregation is not limited to molecules in screening libraries, as biological reagents and even

drugs can also aggregate *in vitro*.<sup>10–17</sup> The potential relevance of aggregation to drug delivery has been suggested by Frenkel et al., who proposed that aggregation facilitates the uptake of non-nucleoside reverse transcriptase inhibitors through absorption by particle-recognizing M cells in Peyer's patches of mucosa-associated lymphoid tissue.<sup>18</sup> Also, aggregates appear to be stable in more biological milieus, such as at high protein concentrations and in cell culture.<sup>19,20</sup> In short, inhibition by aggregation is a common property among biologically interesting organic molecules with widespread effects in biological systems of varying complexity.

- (1) Rishton, G. M. *Drug Discovery Today* **2003**, *8*, 86–96.
- (2) Hann, M. M.; Oprea, T. I. *Curr. Opin. Chem. Biol.* **2004**, *8*, 255–263.
- (3) Roche, O.; Schneider, P.; Zuegge, J.; Guba, W.; Kansy, M.; Alanine, A.; Bleicher, K.; Danel, F.; Gutknecht, E. M.; Rogers-Evans, M.; Neidhart, W.; Stalder, H.; Dillon, M.; Sjogren, E.; Fotouhi, N.; Gillespie, P.; Goodnow, R.; Harris, W.; Jones, P.; Taniguchi, M.; Tsujii, S.; von der Saal, W.; Zimmermann, G.; Schneider, G. *J. Med. Chem.* **2002**, *45*, 137–142.
- (4) DeWitte, R. S. *Drug Discovery Today* **2006**, *11*, 855–859.
- (5) Keseru, G. *Drug Discovery Today* **2006**, *11*, 741–748.
- (6) Walters, W. P.; Ajay; Murcko, M. A. *Curr. Opin. Chem. Biol.* **1999**, *3*, 384–387.
- (7) Veber, D. F.; Johnson, S. R.; Cheng, H. Y.; Smith, B. R.; Ward, K. W.; Kopple, K. D. *J. Med. Chem.* **2002**, *45*, 2615–2623.
- (8) McGovern, S. L.; Caselli, E.; Grigorieff, N.; Shoichet, B. K. *J. Med. Chem.* **2002**, *45*, 1712–22.
- (9) Feng, B.; Simeonov, A.; Jadhav, A.; Babaoglu, K.; Inglese, J.; Shoichet, B.; Austin, C. *J. Med. Chem.* **2007**, *50*, 2385–90.

- (10) McGovern, S. L.; Shoichet, B. K. *J. Med. Chem.* **2003**, *46*, 1478–1483.
- (11) Seidler, J.; McGovern, S. L.; Doman, T.; Shoichet, B. K. *J. Med. Chem.* **2003**, *46*, 4477–4486.
- (12) Liu, H.; Wang, Z.; Regni, C.; Zou, X.; Tipton, P. A. *Biochemistry* **2004**, *27*, 8662–8669.
- (13) Davies, S.; Reddy, H.; Caviano, M.; Cohen, P. *Biochem. J.* **2000**, *351*, 95–105.
- (14) Turk, B. *Nat. Rev. Drug Discovery* **2006**, *5*, 785–799.
- (15) Reddie, K.; Roberts, D.; Dore, T. *J. Med. Chem.* **2006**, *49*, 4857–4860.
- (16) Lingameneni, R.; Vysotskaya, T.; Duch, D.; Hemmings, H. *FEBS Lett.* **2000**, *473*, 265–268.
- (17) Lipinski, C. A.; Lombardo, F.; Dominy, B. W.; Feeney, P. J. *Adv. Drug Delivery Rev.* **1997**, *23*, 3–25.
- (18) Frenkel, Y. V.; Clark, A. D. J.; Das, K.; Wang, Y.-H.; Lewi, P. J.; Janssen, P. A. J.; Arnold, E. *J. Med. Chem.* **2005**, *48*, 1974–1983.
- (19) Coan, K. E.; Shoichet, B. K. *Mol. Biosyst.* **2007**, *3*, 208–213.
- (20) Feng, B. Y.; Shoichet, B. K. *Nat. Chem. Biol.* **2008**, *4*, 197–199.

Despite their prevalence, the basic principles of aggregate formation and activity remain obscure. The signatures of aggregate behavior are well known: reversal by nonionic detergent, steep dose–response curves, and acute sensitivity to enzyme concentration, which have assisted the rapid identification of aggregate-based inhibition.<sup>21–26</sup> In contrast, we have had no way to measure something as elementary as the concentration of the aggregate particles. Were we able to measure this concentration, we could begin to explore several fundamental properties of aggregates. What is the stoichiometry of the aggregate–enzyme interaction? Are aggregates in equilibrium with soluble monomer? Are aggregates hollow or solid? Addressing these questions is essential to understanding aggregate structure and mechanism.

Here we measure particle concentrations for known aggregating molecules, using flow cytometry to count the number of particles in a specific volume. By correlating enzyme inhibition with aggregate count, we estimate the stoichiometry and affinity of the binding interaction. We further investigate the point at which aggregates begin to form, the “critical aggregation concentration” (CAC), showing that aggregate count increases linearly with added monomer above the CAC. To determine whether monomer concentration is constant above the CAC, analogous to a critical micelle concentration, we quantified the amount of compound in the aggregate and monomer forms, which were separated by centrifugation. In combination with size measurements and computed volumes for the individual monomers, we deduce that aggregates are densely packed particles. These results expand our fundamental understanding of aggregate behavior and provide insight into the structure, affinity, and mechanism of this ubiquitous inhibitory species.

## Experimental Section

**Materials.** AmpC  $\beta$ -lactamase was expressed and purified as previously described.<sup>27</sup> Tetraiodophenolphthalein (TIPT), nicardipine, staurosporine aglycone (K252c), latex beads at 110, 200, 310, 460, and 620 nm, and Triton X-100 were purchased from Sigma-Aldrich. Miconazole was purchased from ICN and L-755,507 from Tocris. Trifluralin and cinnarizine were gifts from Dr. Joe Goodwin at BD Biosciences. AlignFlow flow cytometry beads at 2.5  $\mu$ m were purchased from Invitrogen. Centa was purchased from CalBiochem. All materials were used as supplied by the manufacturer.

**Flow Cytometry.** Particle characterization was performed using a BD Gentest Solubility Scanner, a flow cytometer optimized for the detection of insoluble particles. Mixtures were made in a 96-well plate with a final volume of 200  $\mu$ L/well. All buffers were filtered with a 0.22  $\mu$ m filter prior to use. Aggregating compounds were diluted into 50 mM potassium phosphate (KPi), pH 7.0, at room temperature, from concentrated stocks in DMSO. For TIPT, K252c, cinnarizine, and trifluralin, the final concentration of DMSO was 0.5%. For L-755,507, the final concentration of DMSO was 1%. To reduce error, solutions of 50  $\mu$ M nicardipine and 10  $\mu$ M miconazole in 0.1% DMSO were made and serially diluted into 50 mM KPi buffer containing 0.1% DMSO. All solutions were

mixed gently by pipet  $\sim$ 5 s after the addition of compound, and measurements were begun immediately thereafter. Each concentration was measured in at least triplicate. The background count of buffer with DMSO in the absence of compound was measured for each data set, and this value was subtracted from each measurement in the set. The counting accuracy of the flow cytometer was calibrated using latex beads at sizes 110, 200, 310, 460, and 620 nm and Nile Red calibration beads at 2.49  $\mu$ m. We compared the known bead concentration to that measured by the flow cytometer and determined that, for particles with size distributions above 300 nm in diameter, the flow cytometer undercounted the bead concentration by 2.85-fold (the average error for beads greater than 300 nm). To account for this undercounting, all particle counts were multiplied by a correction factor of 2.85. For particles below 300 nm, the counting accuracy of the flow cytometer deteriorated rapidly, and so we estimated an upper limit based on a correction factor of 2000. This factor was determined on the basis of the maximum error observed (1000-fold at 100 nm) and the fact that we only observed about half of the size distribution, since the flow cytometer does not measure particles below 100 nm. Measurements were acquired for 3 s with a flow rate of 0.5  $\mu$ L/s using a 3 mW laser at 635 nm. Photon signatures were collected at 90° with a PMT setting of 99 and the threshold channel set to 25.

**$\beta$ -Lactamase Assays.**  $\beta$ -Lactamase activity and inhibition were monitored in 50 mM KPi buffer, pH 7.0, at room temperature. The substrate centa was prepared as a 12.5 mM stock in 50 mM KPi buffer. DMSO stocks of aggregating inhibitors nicardipine and miconazole were prepared so that the final concentration of DMSO was 0.1%. IC<sub>50</sub> values for the other compounds were measured at the indicated concentrations of DMSO (Table 1). Each concentration of inhibitor was measured in triplicate for miconazole and nicardipine and in duplicate for the rest of the compounds. Results were controlled for the effect of DMSO on enzyme rates. Inhibitor and 2.3 nM  $\beta$ -lactamase were incubated for 5 min, and the reaction was initiated by the addition of 125  $\mu$ M centa substrate. Change in absorbance was monitored at 405 nm for 100 s.

**Dynamic Light Scattering.** The aggregators miconazole and nicardipine were delivered from concentrated DMSO stocks into filtered 50 mM KPi buffer, pH 7.0, at room temperature for a final concentration of 0.1% DMSO. Measurements were made using a DynaPro MS/X with a 55 mW laser at 826.6 nm, using a detector angle of 90°. The laser power was 100%, and the integration time was 200 s. Data were filtered using a maximum sum of squares difference (SOS) of 100 and a baseline limit of  $1 \pm 0.01$ . Histograms represent the average of three independent data sets, each with at least 10 measurements.

**Determination of Monomer and Aggregate Concentrations.** Solutions of nicardipine, K252c, and TIPT were prepared at multiple concentrations by diluting concentrated DMSO stocks into 50 mM KPi, pH 7.0. The final amount of DMSO at each concentration was 0.1% for nicardipine, 0.5% for K252c, and 5% for TIPT. Solutions were mixed gently and then centrifuged at 16000g for 1 h. After centrifugation, the supernatant was collected and analyzed by flow cytometry to determine that there were no detectable aggregates remaining in solution. The bottom 10  $\mu$ L (from a starting volume of 1 mL) was considered the pellet and resuspended in pure DMSO. UV–visible spectrophotometry was used to determine the concentration of compound in the supernatant and the resuspended pellet. Each concentration was prepared and measured in triplicate. Absorbance was measured at 355 nm for the nicardipine supernatant (0.1% DMSO in 50 mM KPi,  $\epsilon = 6.3 \times 10^3 \text{ M}^{-1} \text{ cm}^{-1}$ ) and 352 nm for the pellet (1% KPi in pure DMSO,  $\epsilon = 6.0 \times 10^3 \text{ M}^{-1} \text{ cm}^{-1}$ ). Absorbance was measured at 372 nm for the K252c supernatant (0.5% DMSO in 50 mM KPi,  $\epsilon = 5.5 \times 10^3 \text{ M}^{-1} \text{ cm}^{-1}$ ) and 335 nm for the pellet (1% KPi in pure DMSO,  $\epsilon = 1.8 \times 10^4 \text{ M}^{-1} \text{ cm}^{-1}$ ). The TIPT supernatant was lyophilized overnight and resuspended in 1% KPi in pure DMSO. Absorbance was measured at 337 nm for the TIPT supernatant and pellet (1% KPi in pure DMSO,  $\epsilon = 1.3 \times 10^4 \text{ M}^{-1} \text{ cm}^{-1}$ ).

(21) McGovern, S. L.; Helfand, B. T.; Feng, B. Y.; Shoichet, B. K. *J. Med. Chem.* **2003**, *46*, 4265–4272.

(22) Shoichet, B. K. *J. Med. Chem.* **2006**, *49*, 7274–7277.

(23) Feng, B. Y.; Shoichet, B. K. *Nat. Protocols* **2006**, *1*, 550–553.

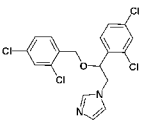
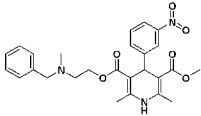
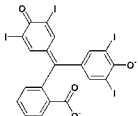
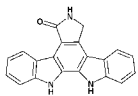
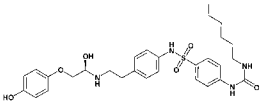
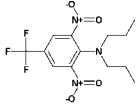
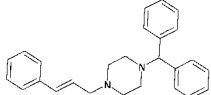
(24) Feng, B. Y.; Shelat, A.; Doman, T. N.; Guy, R. K.; Shoichet, B. K. *Nat. Chem. Biol.* **2005**, *1*, 146–148.

(25) Ryan, A. J.; Gray, N. M.; Lowe, P. N.; Chung, C. W. *J. Med. Chem.* **2003**, 3448–3451.

(26) Giannetti, A. M.; Koch, B. D.; Browner, M. F. *J. Med. Chem.* **2008**, *51*, 574–580.

(27) Weston, G. S.; Blazquez, J.; Baquero, F.; Shoichet, B. K. *J. Med. Chem.* **1998**, *41*, 4577–4586.

**Table 1.** Characteristics of Aggregating Inhibitors Measured by Flow Cytometry

Compound	IC <sub>50</sub> vs. $\beta$ -lactamase ( $\mu$ M)	CAC ( $\mu$ M)	Total Organic Molecule ( $\mu$ M)	Aggregate Concentration (fM)	Diameter (nm)
Miconazole 	25 <sup>a</sup>	3 $\pm$ 2	4-9	5-27	394
Nicardipine 	66 <sup>a</sup>	32 $\pm$ 3	34-44	6-28	569
TIPT 	5 <sup>b</sup>	10 $\pm$ 2	NM <sup>d</sup>	NM <sup>d</sup>	140
K252c 	8 <sup>b</sup>	4 $\pm$ 2	NM <sup>d</sup>	NM <sup>d</sup>	150
L-755,507 	3 <sup>c</sup>	6 $\pm$ 2	6-11	<10 pM	150
Trifluralin 	7 <sup>b</sup>	3 $\pm$ 2	2-5	<10 pM	140
Cinnarizine 	40 <sup>b</sup>	7 $\pm$ 3	7-10	<10 pM	150

<sup>a</sup> 0.1% DMSO. <sup>b</sup> 0.5% DMSO. <sup>c</sup> 1% DMSO. <sup>d</sup> Not measured.

**Calculations.** The Mitools toolkit (molinspiration.com) was used to calculate the molecular volume for each compound, which was multiplied by the number of monomers per aggregate to determine a calculated volume for the aggregate. The dimensions of a molecule of AmpC  $\beta$ -lactamase were determined using PyMOL and PDB structure 1KE9.

## Results

To determine the concentration of the aggregate species, we counted aggregate particles in a known volume using the BD Gentest Solubility Scanner, a flow cytometer specifically optimized for counting and characterizing aggregate particles using light scattering.<sup>28</sup> We chose seven known aggregators: miconazole, nicardipine, tetraiodophenolphthalein (TIPT), staurosporine aglycone (K262c), L-755,507, cinnarizine, and trifluralin (Table 1). For each compound, we tested a range of concentrations until we began to observe particle formation, indicated by an increase in the intensity of scattered light. Once the total concentration of small molecules passed this threshold (the CAC), we observed a sharp and linear increase in the number of particles (Figure 1). For instance, below 30  $\mu$ M nicardipine, an insignificant number of particles were detected

by the flow cytometer (Figure 1A). Above 32  $\mu$ M of the monomer, the number of particles increased steadily at a rate of nearly 10 000 particles for every 5  $\mu$ M increase in the concentration of the organic molecule (in a volume of 1.5  $\mu$ L). To minimize error, these concentrations were created by serial dilution; however, similar relationships were observed when each concentration was made individually (data not shown). As a practical note, the CAC could vary dramatically for a given molecule, depending on the composition of the buffer, particularly with respect to the DMSO concentration. In extreme cases, we observed as much as a 10-fold change in the CAC. For example, the CAC for TIPT went from  $\sim$ 1 to  $\sim$ 10  $\mu$ M when going from 0.1% to 1% DMSO (data not shown).

Simply using the known volume of the sample, we used these particle counts to calculate the particle concentration. For nicardipine and miconazole, which form particles between 300 and 600 nm in diameter, we found that the particle concentration just above the CAC ranged from 5 to 30 fM, nearly 10<sup>9</sup>-fold lower than the concentration of the monomeric small molecule (Table 1). For smaller aggregates, such as those composed of trifluralin, cinnarizine, TIPT, and L-755,507 (with diameters around 150 nm), the particle count increased much more rapidly, quickly surpassing the detection limits of the instrument and preventing more detailed analysis. In addition, for particles less

(28) [http://www.bdbiosciences.com/discovery\\_labware/products/display\\_product.php?keyID=242](http://www.bdbiosciences.com/discovery_labware/products/display_product.php?keyID=242)

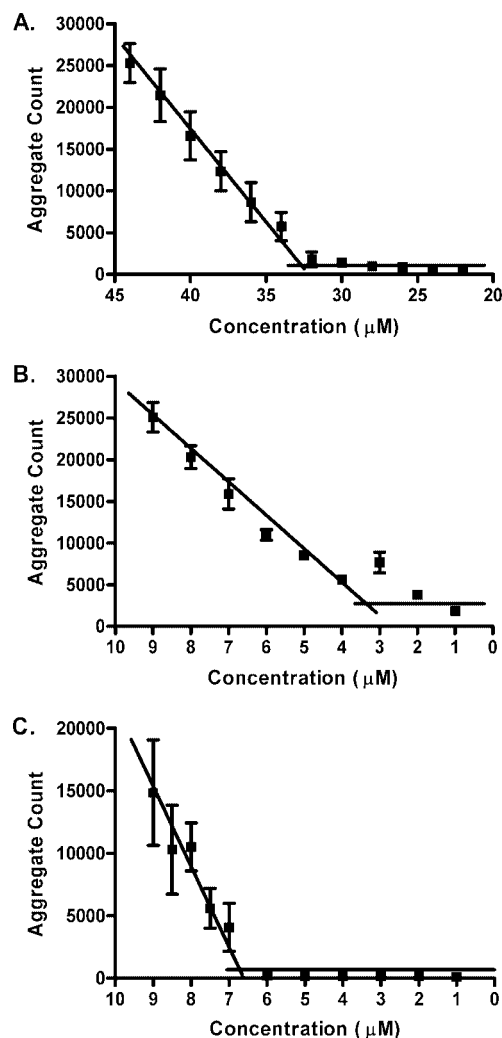


**Figure 1.** Critical aggregation points of (A) nicardipine at 0.1% DMSO, (B) miconazole at 0.1% DMSO, and (C) L-755,507 at 1% DMSO in 1.5  $\mu\text{L}$  of 50 mM potassium phosphate buffer, measured using flow cytometry. For (A) and (B), solutions were made by serial dilution, while compound was added directly for (C). Concentrations are represented as the mean and standard deviation of at least three replicates.

than 300 nm in diameter, the flow cytometer grossly undercounts the number of particles. We therefore multiplied the observed number of particles by a factor of 2000 to estimate the upper limit for the particle count, resulting in low picomolar concentrations. Whereas we believe the concentrations of miconazole and nicardipine aggregates to be accurate, those for the smaller particles must be considered conservative estimates.

Knowing these particle concentrations enabled us to determine the stoichiometry of the aggregate–enzyme interaction for the two aggregators, nicardipine and miconazole, for which we had accurate concentrations. By assuming that percent inhibition directly correlates to the percent of bound enzyme, we related the number of bound enzyme molecules to the number of aggregate particles counted by the flow cytometer (Figure 2). To do so, we measured the inhibition of a model enzyme, AmpC  $\beta$ -lactamase, in the presence of directly measurable concentrations of aggregate particles. We chose nicardipine and miconazole because the concentration of these particles increased slowly enough to allow a linear analysis of the particle count versus percent inhibition. Even for nicardipine and miconazole, these aggregate concentrations corresponded only to inhibition that ranged from 0 to about 30%. To estimate the aggregate

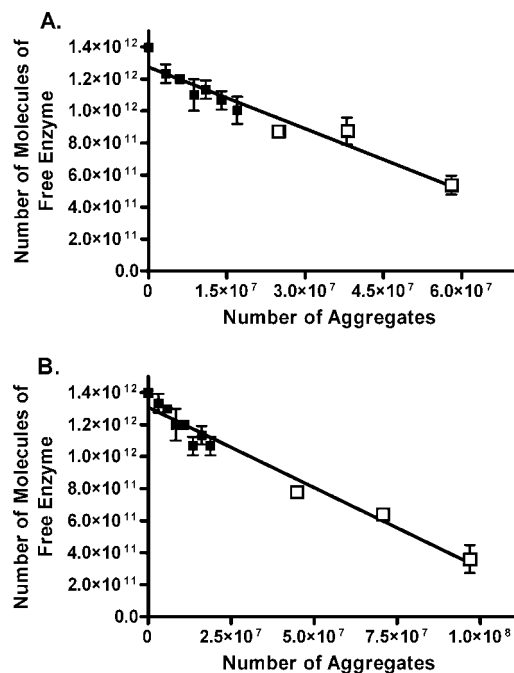


**Figure 2.** Correlation of  $\beta$ -lactamase inhibition to aggregate count for (A) nicardipine and (B) miconazole at 0.1% DMSO. The number of molecules of free enzyme is calculated as the product of percent activity and the total amount of enzyme in 1 mL. Aggregate count is measured by flow cytometry in a volume of 1.5  $\mu\text{L}$  and extrapolated for 1 mL. Empty boxes represent aggregate counts that were extrapolated on the basis of a linear regression analysis of the measured aggregate count data points because the count was above the detection limit of the flow cytometer at higher concentrations of aggregating molecule. Free enzyme values are represented as the mean and standard deviation of three replicates. Aggregate counts are the mean of at least five measurements.

concentration at the  $\text{IC}_{50}$ , we extrapolated the ratio between added organic molecule and particle concentration (Figure 2). Since inhibition is linearly related to the concentration of organic molecule and there is a linear relationship between inhibition and particle count through 30% inhibition, we assume that a linear model is adequate for extrapolating the particle count. Over the measured concentrations, the slopes of the inhibition versus particle graphs represent the number of molecules of enzyme bound per aggregate:  $12\,850 \pm 875$  for nicardipine and  $10\,040 \pm 440$  for miconazole.

One long-standing question has been whether enzyme is adsorbed to the aggregate surface or absorbed into the aggregate. To address this, we next determined whether the calculated number of bound enzyme molecules could even fit upon the surface of the aggregate. If the surface area is insufficient to accommodate all of the bound enzyme, this would suggest that absorption into the aggregate is necessary. To be conservative, we chose the smallest principle dimension of the model protein to calculate the volume of a shell around an aggregate, representing the minimum volume available to surface-bound enzyme (the smallest principle dimension of AmpC is 3.7 nm). We calculated the volume of a 3.7 nm shell around an aggregate of nicardipine or miconazole. We then compared this volume to the total volume of 12 850 or 10 040 enzyme molecules (for nicardipine and miconazole, respectively), modeled as rectangles with dimensions equal to the principle dimensions of an AmpC molecule. When we compared these two volumes, we found that there was more than enough room to accommodate all enzyme molecules on the surface of the aggregate. The total volume of enzyme bound is only 16% of the total volume

available in a 3.7 nm shell around a nicardipine particle (diameter 569 nm) and 26% of a shell around a miconazole particle (diameter 394 nm).

In measuring the CAC, we found that aggregation is fully reversible if the aggregates are diluted below their CACs (Figure 1). For example, at 40  $\mu\text{M}$  nicardipine, there are approximately 16 000 particles; however, at half that concentration, 20  $\mu\text{M}$ , the count has returned to the background count of around 1000, showing that the aggregates will dissociate if diluted below the CAC ( $\sim 33 \mu\text{M}$  for nicardipine). This reversibility resembles micelle behavior, and so we looked for other behavior we would expect on the basis of micelle theory.<sup>29,30</sup> For micelles, the linear increase in particle count beyond the CMC is due to two factors: (a) the concentration of free monomer will never go higher than the CMC and all monomeric molecules added beyond the CMC will form micelles, and (b) the micelles formed are uniform in their size distribution across increasing concentrations.

To investigate monomer concentration above the CAC, we looked at three compounds that had relatively strong UV–visible absorbance spectra: nicardipine, K252c, and TIPT. To quantify the monomer and aggregate phases, we centrifuged aqueous solutions of varied concentrations of aggregating molecules and separated the supernatant and pellet. After 1 h of centrifugation, no aggregates were detectable in the supernatant, as measured by flow cytometry, indicating that the supernatant represented the monomeric fraction. The pellet (representing the aggregate fraction) was resuspended in DMSO, and the concentrations of monomer (supernatant) and aggregate (pellet) were measured spectrophotometrically. For each compound tested, the concentration in the supernatant remained constant above the CAC, while the aggregate concentration (the pellet) increased steadily, suggesting that all additional compound above the CAC forms aggregates (Figure 3). We also found that the size distribution of the particles remained fairly constant as the concentration of compound was raised above the CAC, at least to the detection limit of the instrument (Figure 4). Dynamic light scattering confirmed that there was no significant population smaller than 100 nm, which is below the detection limit of the flow cytometer (Figure 4 insets).

Since aggregate count increased linearly and all monomer beyond the CAC forms aggregates, we could calculate the number of monomers that form each aggregate. For accuracy we again focused on miconazole and nicardipine, which form the largest particles. We graphed the total concentration of small-molecule monomer added versus particle count over the linear range (Figure 1A,B). The resulting slopes represent the average number of monomers that form each aggregate particle:  $4.5 \times 10^8$  monomers per particle for nicardipine and  $2.3 \times 10^8$  monomers per particle for miconazole. Since we knew the sizes of these aggregates by light scattering, and we could calculate the volume of each monomer of organic molecule, we could then calculate how the volume of this number of monomers compared to the measured volume. We divided the particle volumes measured by flow cytometry ( $V_{\text{measured}}$ ) by the calculated total volume of monomers in each aggregate ( $V_{\text{calculated}}$ , calculated monomer volume multiplied by number of monomers per aggregate) (Figure 5). Here,  $V_{\text{calculated}}$  is an estimate of the size of a perfectly packed aggregate, a minimum volume for a solid aggregate. For nicardipine the ratio of  $V_{\text{measured}}/V_{\text{calculated}}$

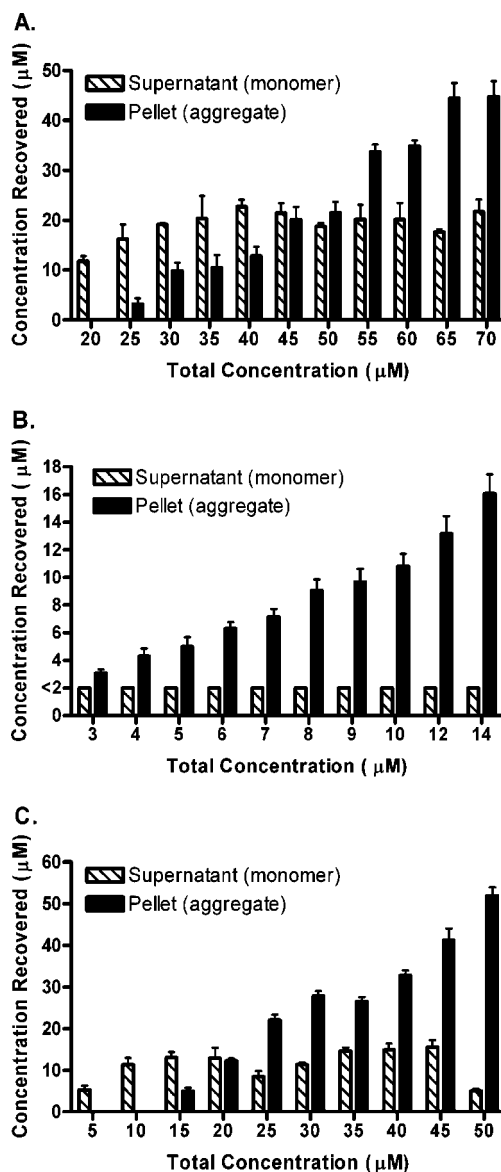


**Figure 3.** Concentration of monomer and aggregate fractions in (A) nicardipine at 0.1% DMSO, (B) K252c at 0.5% DMSO, and (C) TIPT at 5% DMSO in 50 mM KPi buffer. Aggregates were pulled down by centrifugation at 16000g for 1 h. The supernatant was removed, and the concentration of soluble monomer was determined by UV–visible spectrophotometry. The concentration of compound in the aggregate form was determined by resuspending the pellet in DMSO and performing spectrophotometric analysis. Bars represent the mean and standard deviation of three replicate measurements.

was 1.1, and for miconazole the ratio was 0.6. These ratios indicate that the integrated volume of the monomers that make up each particle is sufficient to account for most or all of the measured volume of the particle, suggesting that these aggregates are solidly packed with monomer and inconsistent with the possibility that they might be hollow.

## Discussion

Nonspecific inhibition by aggregation is widespread in early drug discovery, but the properties and mechanism of these aggregates are poorly understood. An impediment has been our inability to simply measure aggregate concentration; overcoming this problem is a key result of this work. The particle concentration just beyond the critical aggregation point is in

(29) Tanford, C. *J. Phys. Chem.* **1974**, *78*, 2469.

(30) Mukerjee, P.; Mysels, K. *J. Natl. Stand. Ref. Data Ser., Natl. Bur. Stand.* **1971**, *36*, 1–227.

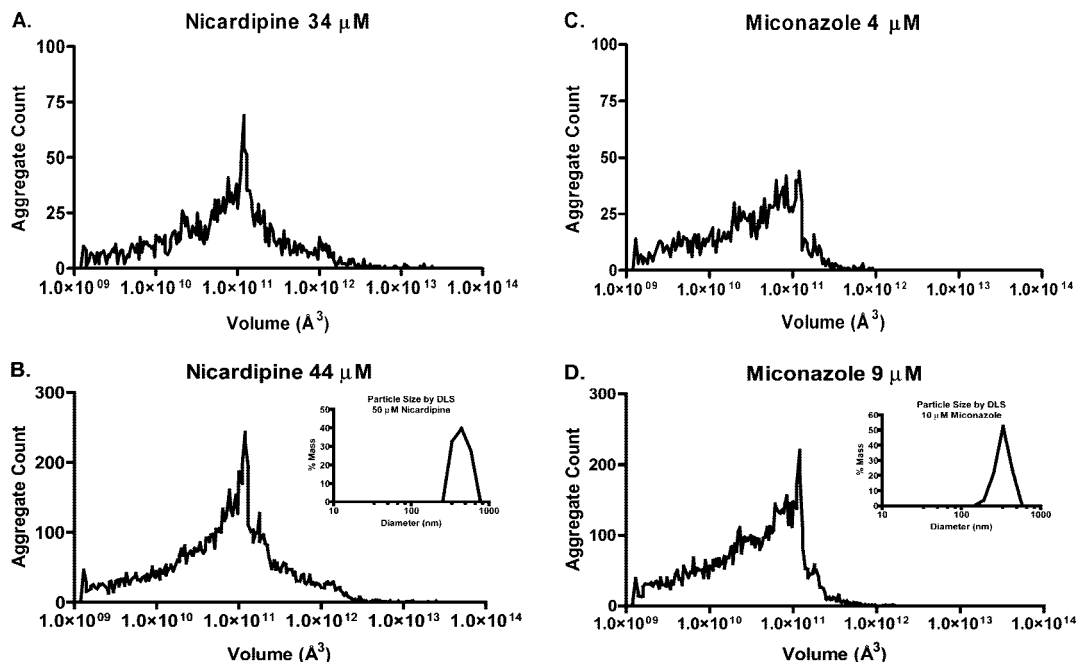


**Figure 4.** Size distribution histograms of (A) 34  $\mu\text{M}$  nicardipine, (B) 44  $\mu\text{M}$  nicardipine, (C) 4  $\mu\text{M}$  miconazole, and (D) 9  $\mu\text{M}$  miconazole determined by flow cytometry. Dynamic light scattering confirmed that there were no particles smaller than 100 nm in diameter, which is below the detection limit of the flow cytometer (inset of B and D). All samples are in filtered 50 mM KPi, 0.1% DMSO.

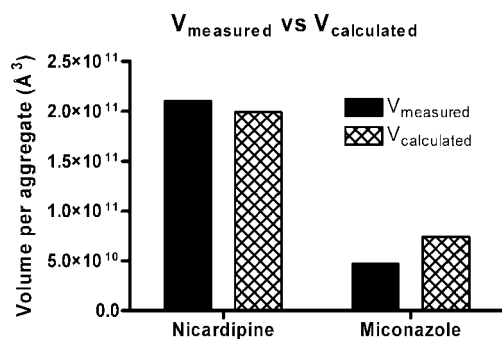


**Figure 5.** Comparison of calculated aggregate volumes to measured volumes for nicardipine and miconazole. Calculated volumes are the product of the molecular volume from Mitools and the predicted number of monomers that form each aggregate. The measured volume is the mean of the size distribution obtained using flow cytometry.

the low femtomolar range (Figure 1, Table 1). From this observation several others follow. First, we investigate the stoichiometry of the enzyme–aggregate interaction and the implications of this to the binding affinity and mechanism. Second, by correlating the amount of added organic material to the rise in particle number we find that large aggregates are composed of  $10^8$  organic monomers, the total volume of which closely matches the measured particle volumes, suggesting that the particles are solid (Figure 5). Finally, we elucidate some of the basic characteristics of aggregate formation, most notably that aggregation is reversible, and in this respect it resembles micelle behavior (Figures 3 and 4).

By correlating enzyme inhibition to particle concentration, we found that larger aggregates, such as miconazole and nicardipine, bound over 10 000 enzyme molecules per aggregate (Figure 2). As outlandish as this stoichiometry is, it is consistent with what we know about aggregate behavior. A distinguishing feature of aggregate-based inhibition is its sensitivity to changes in enzyme concentration. From early studies we knew that increasing enzyme concentration 10-fold eliminated the observed

inhibition, which seemed unprecedented for an inhibitor present at concentrations 1000- to 10 000-fold higher than that of the enzyme.<sup>8,21</sup> Since the stoichiometry of enzyme to aggregate is now shown to be roughly 10 000 to 1, and since the aggregates themselves are present only in the mid-femtomolar range, increasing enzyme concentration simply overwhelms the capacity of the aggregate to sequester enzyme, eliminating inhibition. By first principles, the observation that inhibition is stoichiometric in the low nanomolar concentration range for both enzyme and enzyme-binding sites on the aggregate suggests that the  $K_d$  of this interaction must be at least 2 orders of magnitude, and more likely 3, below these concentrations. Both the high molar ratio and high affinity are consistent with the steep dose–response curves that are often associated with aggregate-based inhibition<sup>9,22</sup> and the low off-rate of enzyme from the aggregates.<sup>19</sup>

Despite this remarkable stoichiometry, we calculate that even 10 000 enzyme molecules can fit comfortably on the surface of the aggregate, supporting an adsorption model for binding. Using transmission electron microscopy, we have previously observed enzyme adsorbed to the surface of aggregate particles; however, it is difficult to determine whether enzyme molecules are absorbed inside the aggregate. Although we still cannot rule out absorption, an adsorption mechanism is consistent with our observations that low concentrations of nonionic detergent can reverse inhibition without disrupting the aggregates themselves and our finding here that aggregate particles are densely packed.

We found that larger aggregates, like those composed of nicardipine or miconazole molecules, contained approximately  $10^8$  small-molecule monomers per aggregate. To our surprise, the calculated total volume based on the number of small molecules per aggregate closely resembled the observed volumes, suggesting the particles are solid (Figure 5). The calculated volume based on the number of molecules per monomer is an estimated minimum, an unrealistic value that assumes perfect packing, yet our measured volumes are within

2-fold of this value. If these particles were hollow, similar to a liposome, we would expect roughly a 10-fold difference between the measured and calculated volumes. Even with errors from compound sticking to the plate and the small percentage of the particles that fell below the accurate counting range of the flow cytometer, both of which reduce the apparent density of the particles, these results suggest that the aggregates are largely solid.

Several physical properties of these promiscuous aggregates also come into focus. It is easy to imagine that these particles are an intermediate form of precipitate, but that does not seem to be the case. Although aggregates can transition to precipitant as concentration is increased, the latter does not sequester protein.<sup>22,24</sup> Consistent with these observations, the particles here appear to be in equilibrium with monomer and are a reversible phase. On lowering the concentration of a suspension of aggregates below its CAC, the particles rapidly redissolve (tens of seconds). As anyone who has tried to dissolve organic material into aqueous solution can attest, this is rarely true for precipitated material, which is why most organic molecules are delivered to aqueous buffer from DMSO stocks. Thus, although the aggregates are only transiently stable, the individual particles appear to approach true equilibrium.

It is appropriate to mention several caveats and remaining gaps. Particle counts made by the BD flow cytometer are only quantitatively reliable for particles in the 400 nm diameter range and larger, and even here they require adjustment against controls. The particle count for smaller particles can only be grossly estimated. Similarly, the stoichiometry of the enzyme–aggregate interaction could only be measured in the early part of the inhibition curve, beyond which we exceed the counting capacity of the instrument. Thus, these results rely on extrapolation, assuming a constant linear correlation. Also, it is possible that not all aggregate-based inhibitors have the same properties and structures as those we have studied here. It is convenient to assume that all promiscuous aggregates will have similar structures and mechanisms, but there is no strong theory to suggest that this is true. Finally, key questions remain unad-

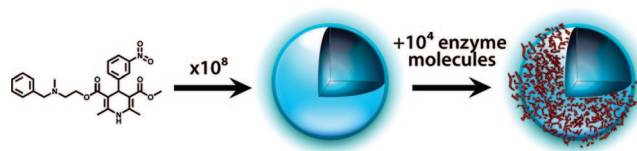


**Figure 6.** Model of aggregate structure and enzyme binding. Some organic molecules can form densely packed particles ( $10^8$  small molecules per aggregate for larger particles) in aqueous media. Once formed, these larger particles sequester and then inhibit enzyme with a stoichiometry of approximately  $10^4$  enzyme molecules per aggregate. The surface of the aggregate is sufficient to accommodate all bound enzyme.

dressed for aggregate mechanism, including why enzyme becomes inhibited when bound to an aggregate.

These caveats, while important, do not diminish our confidence in the main conclusions of this study, which suggest the following model (Figure 6). At micromolar concentrations, organic molecules can reversibly associate into colloid-like particles in aqueous media. For larger particles, about  $10^8$  small-molecule monomers associate per particle. These particles are densely packed and, again for larger particles, sequester about  $10^4$  enzyme molecules each. Whereas we cannot rule out the possibility that enzyme is absorbed inside the aggregate, adsorption to the surface is sufficient to accommodate all bound enzyme. This model, though still crude, provides a foundation for future studies into these ubiquitous but often confounding particles.

**Acknowledgment.** This work was supported by NIH grant GM71630 (to B.K.S.). K.E.C. was partly supported by NIH grant T32-GM64337 (C. Craik, PI) and by a fellowship in the field of Pharmaceuticals awarded by the PhRMA Foundation. We thank Dr. J. Goodwin at BD Biosciences for the generous loan of the BD Gentest Solubility Scanner and for helpful discussions. We also thank A. McReynolds for  $\beta$ -lactamase purification, D. Teotico for PyMOL calculations, and J. Irwin and J. Hert for Molinspiration calculations. We also thank R. Ferreira, V. Thomas, D. Teotico, M. Keiser, and J. Irwin for reading this manuscript.

JA802977H